Malaysian Journal of Mathematical Sciences 14(S) December: 1–13 (2020)
Special Issue: 2nd International Conference on Applied & Industrial Mathematics and Statistics 2019 (ICoAIMS 2019)

MALAYSIAN JOURNAL OF MATHEMATICAL SCIENCES

Journal homepage: http://einspem.upm.edu.my/journal

Paired Solutions of the Jeffery-Hamel Channel Flow Utilizing Nanoparticles in a Kerosene

Naganthran, K. *[1], Md Basir, M. F.[2], Nazar, R.[1], and Md Ismail, A. I.[3]

[1]*Department of Mathematical Sciences, Faculty of Science and Technology, Universiti Kebangsaan Malaysia, Malaysia*
[2]*Department of Mathematical Sciences, Faculty of Science, Universiti Teknologi Malaysia, Malaysia*
[3]*School of Mathematical Sciences, Universiti Sains Malaysia, Malaysia*

E-mail: kohi_kk@yahoo.com
* *Corresponding author*

Received: 15 January 2020
Accepted: 30 July 2020

ABSTRACT

Jeffery-Hamel flow is notable for the applications in the high-current arc in plasma generators, chemical vapour deposition reactors and expanding/contracting regions in industrial machines. The current study is devoted to present the paired solutions of the classical Jeffery-Hamel flow from a source or sink vent within the convergent/divergent channels in a kerosene-based nanofluid which contains copper as the nanoparticle. The suitable similarity transformations are applied to obtain the governing boundary layer equations in the form of ordinary differential equations. The MATLAB solver bvp4c function solved the model efficiently and gave all the numerical results as the parameters vary. The existence of paired solutions is noticeable at a certain range of the channel angle. The increment in the nanoparticle volume fractions found to be delaying the flow separations.

Keywords: Convergent/Divergent channel, Jeffery-Hamel flow, nanofluid, paired solutions.

1. Introduction

The conventional Jeffery-Hamel flow has been developed by Jeffery (1915) and Hamel (1917). Jeffery-Hamel flow involves the two-dimensional incompressible fluid flow between two non-parallel converging /diverging walls which are detached by a specific angle. This particular flow managed to attract the researchers' attention because it is one of the sporadic exact solutions to the Navier-Stokes equations. Jeffery-Hamel flow has wide applications in chemical, mechanical and biomechanical engineering (Turkyilmazoglu (2014)). For instance, the applications include chemical vapour deposition (CVD) reactors, expanding/contracting sections in industrial machines, gas compressors, high-current arc in plasma generators and pipe sections (see Turkyilmazoglu (2014), Fitzjohn and Holstein (1990), Belevtsev et al. (2000)). Meanwhile, Rosenhead (1940), Millsaps and Pohlhausen (1953) and Riley (1989) are those important works which have contributed to the improvement of the classical Jeffery-Hamel flow, theoretically. The existence of the non-uniqueness solutions has been discovered by Fraenkel and Squire (1962) in the Jeffery-Hamel flow symmetrical channels where the walls are marginally curved. Although some of the theories failed in Fraenkel and Squire (1962), the presence of non-uniqueness solutions and separation point gave a hint that the separation flow is a possible occurrence in the Jeffery-Hamel flow.

The work by Fraenkel and Squire (1962) has mainly motivated the contribution of the present investigation in identifying the right non-uniqueness solutions. The study about the nanofluid as the brilliant fluid which conquers many practical applications in high technology industries such as microelectronics, transportation, manufacturing and metrology has been initiated by Choi and Eastman (1995). It is a base fluid with the suspension of nanometer-sized (less than 100nm) solid particles (Das et al. (2007)). The examples of the base fluids in a nanofluid are water, ethylene glycol, pump oil and glycerol (Das et al. (2007)). The valuable works of Moradi et al. (2013), Petroudi et al. (2014), Sheikholeslami et al. (2012) and Usman et al. (2018) have incorporated nanofluid in the Jeffery-Hamel flow. Moradi et al. (2015) solved the problem of the Jeffery-Hamel flow and heat transfer analytically by considering the effect of viscous dissipation in nanofluids containing a different type of nanoparticles (copper, alumina and titania). The differential transformation method (DTM) has been used by Moradi et al. (2015) and produced unique solutions only. Therefore, the present study attempts to extend the work of

Moradi et al. (2015) by solving the problem numerically via the bvp4c function in the MATLAB software and present the availability of the paired solutions. The contribution of the present work is highly novel because previously no one had discovered the paired solutions in the Jeffery-Hamel nanofluid flow. The present study is also important in revealing the flow separation points as the governing parameters vary.

2. Problem formulations

Examine the flow from a source/sink at the intersection between two solid walls that meet at an angle $2\alpha_0$ in a kerosene-based nanofluid containing copper (Cu) nanoparticles as it is illustrated in Figure 1, where α_0 is the angle between the two plates. The flow is steady, incompressible and viscous. The

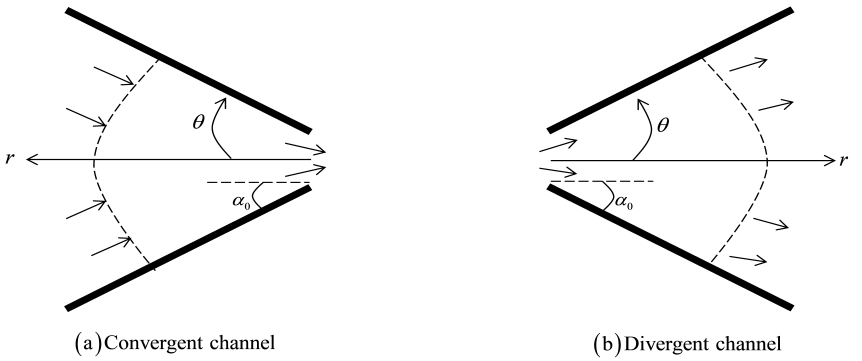

Figure 1: Physical configuration of the problem.

converging/diverging channel wall does not contain the slip condition because the channel is macro-scaled (see Freidoonimehr and Rashidi (2015)). It is assumed that there are no changes in the $z-$ direction because the fluid motion is purely in a radial direction. Hence, the plane polar coordinates (r, θ) are considered and the velocity components can be written as $\mathbf{v}=(u(r,\theta),0)$. The effect of viscous dissipation is considered in the present study. Based on these assumptions, the governing boundary layer flow equations and heat transfer can be formed as follows (see Moradi et al. (2015)):

$$\frac{\rho_{nf}}{r}\frac{\partial(ru)}{\partial r}=0, \tag{1}$$

$$u\frac{\partial u}{\partial r}=-\frac{1}{\rho_{nf}}\frac{\partial p}{\partial r}+\frac{\mu_{nf}}{\rho_{nf}}\left(\frac{\partial^2 u}{\partial r^2}+\frac{1}{r}\frac{\partial u}{\partial r}+\frac{1}{r^2}\frac{\partial^2 u}{\partial \theta^2}-\frac{u}{r^2}\right), \tag{2}$$

$$-\frac{1}{\rho_{nf}r}\frac{\partial p}{\partial \theta}+\frac{\mu_{nf}}{\rho_{nf}}\frac{2}{r^2}\frac{\partial u}{\partial \theta}=0, \tag{3}$$

$$u\frac{\partial T}{\partial r}=\alpha_{nf}\left(\frac{\partial^2 T}{\partial r^2}+\frac{1}{r}\frac{\partial T}{\partial r}+\frac{1}{r^2}\frac{\partial^2 T}{\partial \theta^2}\right)+\frac{\mu_{nf}}{(\rho C_p)_{nf}}\left[4\left(\frac{\partial u}{\partial r}\right)^2+\frac{1}{r^2}\left(\frac{\partial u}{\partial \theta}\right)^2\right], \tag{4}$$

subject to the conditions at the channel centerline, $\theta = 0$

$$\frac{\partial u}{\partial \theta}=0, \qquad \frac{\partial T}{\partial \theta}=0, \qquad u(r,\theta)=U, \tag{5}$$

and the conditions at the wall of the channel, $\theta = \alpha_0$

$$u(r,\theta)=0, \qquad T=T_w, \tag{6}$$

where u is the velocity component in the radial direction, r is the radial direction in cylindrical polar coordinate, ρ_{nf} denotes the density of the nanofluid, μ_{nf} is the viscosity of the nanofluid, θ signifies the tangential direction in the cylindrical polar coordinate, T is the temperature, α_{nf} is the thermal diffusivity of the nanofluid, and $(C_p)_{nf}$ is the specific heat capacity of the nanofluid. The definition of ρ_{nf} and μ_{nf} are given as

$$\rho_{nf}=(1-\phi)\rho_f+\phi\rho_s, \qquad \mu_{nf}=\frac{\mu_f}{(1-\phi)^{2.5}}, \tag{7}$$

where ϕ symbolizes the solid volume fraction of the nanofluid, μ_f is the viscosity of the base fluid (kerosene), ρ_f is the density of the kerosene, and ρ_s represents the density of the solid particles. According to Brinkman (1952), μ_{nf} can be estimated as μ_f which contains suspended dilute fine spherical particles. Next, the thermal diffusivity (α_{nf}) can be defined as

$$\alpha_{nf}=\frac{k_{nf}}{(\rho C_p)_{nf}}, \tag{8}$$

where k_{nf} is the thermal conductivity of the nanofluid and $(\rho C_p)_{nf}$ is the heat capacity of the nanofluid. The following expressions communicates the relations of k_{nf} and $(\rho C_p)_{nf}$ in the present problem (see Pop et al. (2016))

$$\frac{k_{nf}}{k_f}=\frac{(k_s+2k_f)-2\phi(k_f-k_s)}{(k_s+2k_f)+\phi(k_f-k_s)}, \quad (\rho C_p)_{nf}=(1-\phi)(\rho C_p)_f+\phi(\rho C_p)_s, \tag{9}$$

where k_f and k_s are the thermal conductivities of fluid and the solid particles, respectively, and $(\rho C_p)_s$ is the heat capacity of the solid.

By integrating the Eq. (1), the following expression can be attained:

$$f(\theta)=ru(r,\theta), \tag{10}$$

where $f(\theta)$ is an arbitrary function of θ. Next, by defining the dimensionless parameters

$$F(\eta) = \frac{f(\theta)}{Ur}, \qquad \eta = \frac{\theta}{\alpha_0}, \qquad \beta(\eta) = \frac{T}{T_w}, \tag{11}$$

the employment of (11) into Eqs. (2) and (3) eliminates the pressure terms and gives the following ordinary differential equations:

$$F''' + 2\alpha_0 Re(1-\phi)^{2.5} A_1 F F' + 4\alpha_0^2 F' = 0, \tag{12}$$

$$\beta'' + \frac{A_2}{A_3(1-\phi)^{2.5}} EcPr(4\alpha_0^2 F^2 + F'^2) = 0, \tag{13}$$

along with the boundary conditions

$$F(0) = 1, \qquad F'(0) = 0, \qquad F(1) = 0, \qquad \beta(1) = 1, \qquad \beta'(0) = 0, \tag{14}$$

where Re is the Reynolds numbers, Ec is the Eckert number and Pr is the Prandtl number. These governing parameters can be defined as

$$\begin{gathered} Re = \frac{rU\rho_f\alpha_0}{\mu_f}, \qquad Pr = \frac{\mu_f (C_p)_f}{k_f}, \qquad Ec = \frac{U^2}{(C_p)_f T_w}, \\ A_1 = 1 - \phi + \phi\frac{\rho_s}{\rho_f}, \qquad A_2 = 1 - \phi + \phi\frac{(\rho C_p)_s}{(\rho C_p)_f}, \qquad A_3 = \frac{k_{nf}}{k_f}. \end{gathered} \tag{15}$$

In the definition of Re, when $\alpha_0 > 0$ and $U > 0$, it connotes the state of a diverging channel while when $\alpha_0 < 0$ and $U < 0$, it reflects the state of a converging channel. The associated physical quantities of interest in the present study are the skin friction coefficient (C_{f_r}) and the local Nusselt number (Nu_r) which can be defined as (see Moradi et al. (2015))

$$C_{f_r} = \frac{\tau_w}{\rho_f U^2}, \qquad Nu_r = \frac{rq_w}{k_f T_w}, \tag{16}$$

where τ_w and q_w indicate the wall shear stress and heat flux along the converging/diverging channel respectively, and are defined as follows:

$$\tau_w = \frac{\mu_{nf}}{r}\left[\frac{\partial u(r,\theta)}{\partial\theta}\right]_{\theta=\alpha_0}, \qquad q_w = \frac{-k_{nf}}{r}\left[\frac{\partial T}{\partial\theta}\right]_{\theta=\alpha_0}. \tag{17}$$

The substitution of (17) into (16) and by using (11), the reduced skin friction coefficient and the reduced local Nusselt number can be attained as

$$\mathrm{Re}_r C_{f_r} = \frac{1}{(1-\phi)^{2.5}} F'(1), \qquad Nu_r = -\frac{A_3}{\alpha_0}\beta'(1), \tag{18}$$

where $\mathrm{Re}_r = \frac{rU\rho_f\alpha_0}{\mu_f}$ is the local Reynolds number.

3. Results and discussion

The reduced version of the mathematical model as in (12)-(14) is solved by using the MATLAB solver bvp4c function. This built-in function applies the collocation method and efficient in solving the boundary value problem even with the poor guesses (see Gladwell et al. (2003)). However, a good initial guess is requisite to obtain the non-uniqueness numerical solutions. All numerical results are produced with a fixed value of the Prandtl number that is $Pr = 18.3$ (kerosene at 323.15K). In this paper, the "paired solutions" term has been introduced. These paired solutions comprise the first and second solutions. The first and second solutions are named as the paired solutions because both solutions meet at one critical point. In this work, α_0 is considered in the radian, and all numerical results are generated by using the values as in Table 1. Table 2 shows the comparison of the numerical results with the previous literature, and there is a good agreement with the digits up to six decimal places. This proves the accuracy of the collocation method in solving a boundary layer problem and able to withstand the spectral-homotopy analysis method which has been employed by Motsa et al. (2010).

Table 1: Thermophysical properties of kerosene and copper (see Khan et al. (2015)).

Properties	Kerosene	Copper
ρ (kg/m^3)	783	8933
(J/kg·K)	2090	385
(W/m·K)	0.145	401

Table 2: Comparison of the numerical values for $F''(0)$ when $Pr = 1, Ec = 0$ and $\alpha_0 = 0.087266463$ rad.

	$Re = 20$	$Re = 60$	$Re = 100$
Motsa et al. (2010)	−2.5271922514	−3.9421402764	−5.8691651109
Turkyilmazoglu (2014)	−2.52719225146	−3.94214027633	−5.86916511095
Present study	−2.52719234127	−3.94214028422	−5.86916511211

Figure 2 presents the variations of $\mathrm{Re}_r C_{f_r}$ against α_0 as ϕ varies. When $\alpha_0 \geq 1.17$, the value of $\mathrm{Re}_r C_{f_r}$ increases as ϕ decreases from 0.05 to 0.005. The decrement in the solid volume fraction of copper (Cu) affects the density of the base fluid, which is kerosene, to decrease. Eventually, this increases the wall shear stress along the diverging channel and results in the increment of the reduced skin friction coefficient. The positive values of $\mathrm{Re}_r C_{f_r}$ when $\alpha_0 \geq 1.17$ indicate that kerosene imposes the drag force on the diverging wall. The second solution is absent when the channel is diverging. When $-2.21 \leq \alpha_0 < 1.17$, the values of $\mathrm{Re}_r C_{f_r}$ (first solution) decline with the decrement of ϕ.

When the value of ϕ is decreasing, the viscosity of the kerosene-based nanofluid decreases and reduces the fluid velocity at the converging channel (see Figure 3). The wall shear stress along a converging channel decreases and $\mathrm{Re}_r C_{f_r}$ declines. However, the second solution within $-2.21 \leq \alpha_0 < 1.17$ conveys an increment in $\mathrm{Re}_r C_{f_r}$ as ϕ decreases. These second solutions indicate the flow with the separations, in which increase the shear stress along the converging wall. As the channel is converging ($-2.21 \leq \alpha_0 < 1.17$), $\mathrm{Re}_r C_{f_r}$ starts to take the negative value and implies the converging wall impels the drag force to the nanofluid. The trend of $\mathrm{Re}_r C_{f_r}$ (first solution) continues to change when $-2.9 \leq \alpha_0 < -2.21$ as the value of $\mathrm{Re}_r C_{f_r}$ increases as ϕ decreases. The second solution in the range of $-2.9 \leq \alpha_0 < -2.21$ shows the decrement of $\mathrm{Re}_r C_{f_r}$ as ϕ decreases. This irregular trend of the solutions is most probably due to the state of the converging channel. The three points, $(1.17, 1.25), (-2.21, -3.37)$ and $(-2.9, 3.7)$ which are highlighted in Figure 2 change the trend of $\mathrm{Re}_r C_{f_r}$ accordingly as ϕ decreases. Figure 2 also exhibits that an increment in ϕ delays the flow separation as the channel is converging.

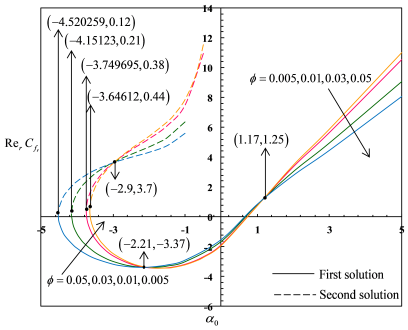

Figure 2: Variations of $\mathrm{Re}_r C_{f_r}$ against α_0 when $Pr = 18.3, Ec = 1.5$ and $Re = 10$ as ϕ varies.

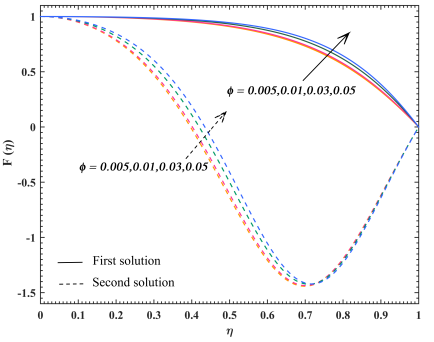

Figure 3: Velocity profiles, $F(\eta)$ when $Pr = 18.3$, $Ec = 1.5$, $\alpha_0 = -2$, and $Re = 10$ for some values of ϕ.

Figure 4 displays the behaviour of Nu_r as ϕ varies along the convergent/ divergent channel. When the channel is diverging, the value of Nu_r increases as ϕ increases. The suspended Cu nanoparticles in the kerosene with a higher thermal conductivity increase the heat flux along the diverging channel. Thus, the rate of heat transfer is enhanced in the diverging channel. The opposite trend can be perceived with the converging channel. Both solutions express the decrement of Nu_r as ϕ increases. Although the thermal conductivity of the nanofluid is high, the converging channel persuades the heat flux to decrease. The temperature profiles as in Figure 5 support the decrement of Nu_r as the nanofluid temperature decreases when ϕ increases in the converging channel.

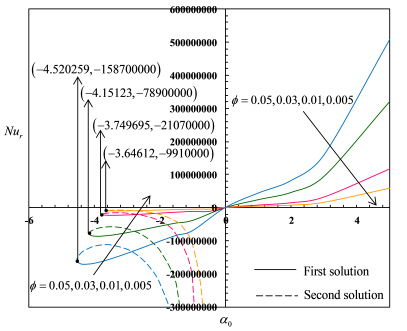

Figure 4: Variations of Nu_r against α_0 when $Pr = 18.3$, $Ec = 1.5$ and $Re = 10$ as ϕ varies.

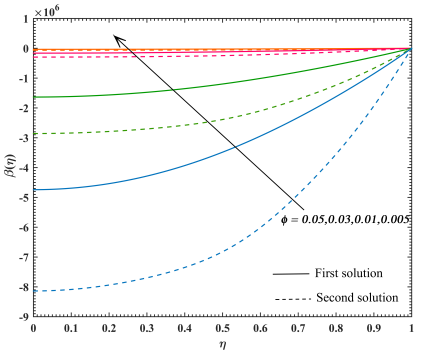

Figure 5: Temperature profiles, $\beta(\eta)$ when $Pr = 18.3, Ec = 1.5, \alpha_0 = -2$, and $Re = 10$ for some values of ϕ.

Figure 6 shows the effect of Ec on Nu_r as the channel is converging/diverging. In a diverging channel, an increment of Ec increases the value of Nu_r. An increment in Ec elucidates more heat dissipates in the fluid flow. Consequently, the rate of heat transfer increases in the diverging channel. On the other hand, the paired solutions in the range of $\alpha_0 < 0$ disclose the deterioration of Nu_r when Ec increases. The converging channel which limits the fluid flow area may reduce the heat flux along the surface, and it is proved by the temperature profiles as in Figure 7 where an increment of Ec reduces the nanofluid temperature in the converging channel. Next, Figure 8 reveals the influence of Re towards $\mathrm{Re}_r C_{f_r}$ as the channel is converging/diverging. Figure 8 also reports the inconsistent patterns as in Figure 2. When $\alpha_0 \geq 2.36$, $\mathrm{Re}_r C_{f_r}$ decreases as Re increases.

An increment of Re increases the inertial forces which reduce the wall shear stress along the diverging channel, hence $\mathrm{Re}_r C_{f_r}$ decreases. The opposite behaviour of $\mathrm{Re}_r C_{f_r}$ is observed as Re increases after $(2.36, 3.37)$. An increment of Re enhanced $\mathrm{Re}_r C_{f_r}$ within $0 \leq \alpha_0 < 2.36$. This may be due to the changes in the width of the channel. The changes in the width of the diverging channel might have contributed to the inconsistency behaviour of $\mathrm{Re}_r C_{f_r}$. Meanwhile, when $\alpha_0 < 0$, the paired solutions exhibit the decrement of $\mathrm{Re}_r C_{f_r}$ as Re increases. Although the increment in Re improves the fluid velocity, the converging channel may reduce the wall shear stress and affects the value of $\mathrm{Re}_r C_{f_r}$ to decline. Figure 9 conveys the increment in the fluid velocity as Re increases. Overall, paired solutions are apparent in the converging channel and variation in ϕ and Re delays the flow separation.

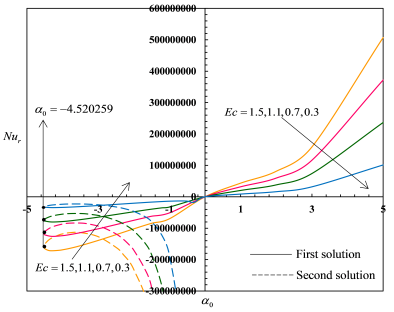

Figure 6: Velocity profiles, $F(\eta)$ when $Pr = 18.3, Ec = 1.5, \alpha_0 = -2$, and $\phi = 0.05$ for some values of Re.

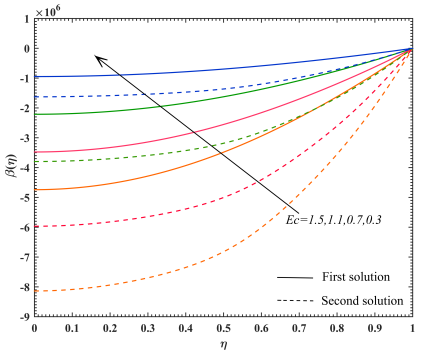

Figure 7: Temperature profiles, $\beta(\eta)$ when $Pr = 18.3, \alpha_0 = -2, \phi = 0.05$ and $Re = 10$ for some values of Ec.

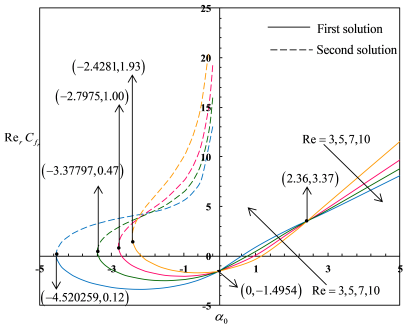

Figure 8: Variations of $\mathrm{Re}_r C_{f_r}$ against α_0 when $Pr = 18.3, Ec = 1.5$ and $\phi = 0.05$ as Re varies.

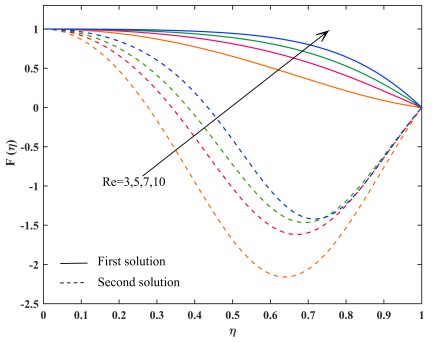

Figure 9: Velocity profiles, $F(\eta)$ when $Pr = 18.3$, $Ec = 1.5$, $\alpha_0 = -2$, and $\phi = 0.05$ for some values of Re.

4. Conclusions

The present study examined the classical Jeffery-Hamel channel flow in a kerosene-based nanofluid containing Cu nanoparticles with the effects of viscous dissipation. The problem has been solved numerically by using the collocation method. It is worth to apply the bvp4c function in the MATLAB as the paired numerical solutions are attainable. The plots of $\mathrm{Re}_r C_{f_r}$ and Nu_r captured interesting behaviours of the paired solutions along a convergent/divergent channel. Few significant points which are found to change the trend of the physical quantities have been accentuated. The paired solutions are observed when the channel is converging, while the unique solution is noticed in the diverging channel. An increment in ϕ and Re managed to delay the flow separation in the converging channel.

Acknowledgements

The work was supported by the university research grants, (GUP-2019-034) from Universiti Kebangsaan Malaysia and (RU Grant 1001/PMATHS/8011 013) from Universiti Sains Malaysia. The author from Universiti Teknologi Malaysia would like to acknowledge the Ministry of Education (MOE) and Research Management Centre-UTM, Universiti Teknologi Malaysia for the financial support given through the research grant (vote number 17J52).

References

Belevtsev, A. A., Isakaev, E. K., Markin, A., Khaimin, V., and Chinnov, V. F. (2000). Analysis of metrological potentialities of a high-current arc in plasma generators with a diverging channel. *High Temperature*, 38(5):667–674.

Brinkman, H. (1952). The viscosity of concentrated suspensions and solutions. *The Journal of Chemical Physics*, 20(4):571–571.

Choi, S. U. and Eastman, J. A. (1995). Enhancing thermal conductivity of fluids with nanoparticles. Technical report, Argonne National Lab., IL (United States).

Das, S. K., Choi, S. U., Yu, W., and Pradeep, T. (2007). *Nanofluids: science and technology*. John Wiley & Sons.

Fitzjohn, J. and Holstein, W. (1990). Divergent flow in chemical vapor deposition reactors. *Journal of the Electrochemical Society*, 137(2):699–703.

Fraenkel, L. E. and Squire, H. B. (1962). Laminar flow in symmetrical channels with slightly curved walls, on the Jeffery-Hamel solutions for flow between plane walls. *Proceedings of the Royal Society of London. Series A. Mathematical and Physical Sciences*, 267(1328):119–138.

Freidoonimehr, N. and Rashidi, M. M. (2015). Dual solutions for MHD Jeffery-Hamel nano-fluid flow in non-parallel walls using predictor homotopy analysis method. *Journal of Applied Fluid Mechanics*, 8(4):911–919.

Gladwell, I., Shampine, L., and Thompson, S. (2003). *Solving ODEs with MATLAB*. Cambridge University Press.

Hamel, G. (1917). Spiralförmige bewegungen zäher flüssigkeiten. *Jahresbericht der deutschen mathematiker-vereinigung*, 25:34–60.

Jeffery, G. (1915). The two-dimensional steady motion of a viscous fluid. *The London, Edinburgh, and Dublin Philosophical Magazine and Journal of Science*, 29(172):455–465.

Khan, U., Ahmed, N., Asadullah, M., and Mohyud-din, S. T. (2015). Effects of viscous dissipation and slip velocity on two-dimensional and axisymmetric squeezing flow of Cu-water and Cu-kerosene nanofluids. *Propulsion and Power Research*, 4(1):40–49.

Millsaps, K. and Pohlhausen, K. (1953). Thermal distributions in Jeffery-Hamel flows between nonparallel plane walls. *Journal of the Aeronautical Sciences*, 20(3):187–196.

Moradi, A., Alsaedi, A., and Hayat, T. (2013). Investigation of nanoparticles effect on the Jeffery–Hamel flow. *Arabian Journal for Science and Engineering*, 38(10):2845–2853.

Moradi, A., Alsaedi, A., and Hayat, T. (2015). Investigation of heat transfer and viscous dissipation effects on the Jeffery-Hamel flow of nanofluids. *Thermal Science*, 19(2).

Motsa, S., Sibanda, P., Awad, F., and Shateyi, S. (2010). A new spectral-homotopy analysis method for the MHD Jeffery–Hamel problem. *Computers & Fluids*, 39(7):1219–1225.

Petroudi, I. R., Ganji, D., Nejad, M. K., Rahimi, J., Rahimi, E., and Rahimifar, A. (2014). Transverse magnetic field on Jeffery–Hamel problem with Cu–water nanofluid between two non parallel plane walls by using collocation method. *Case Studies in Thermal Engineering*, 4:193–201.

Pop, I., Naganthran, K., and Nazar, R. (2016). Numerical solutions of non-alignment stagnation-point flow and heat transfer over a stretching/shrinking surface in a nanofluid. *International Journal of Numerical Methods for Heat & Fluid Flow*, 26(6):1747–1767.

Riley, N. (1989). Heat transfer in Jeffery-Hamel flow. *The Quarterly Journal of Mechanics and Applied Mathematics*, 42(2):203–211.

Rosenhead, L. (1940). The steady two-dimensional radial flow of viscous fluid between two inclined plane walls. *Proceedings of the Royal Society of London. Series A. Mathematical and Physical Sciences*, 175(963):436–467.

Sheikholeslami, M., Ganji, D., Ashorynejad, H., and Rokni, H. B. (2012). Analytical investigation of Jeffery-Hamel flow with high magnetic field and nanoparticle by Adomian decomposition method. *Applied Mathematics and Mechanics*, 33(1):25–36.

Turkyilmazoglu, M. (2014). Extending the traditional Jeffery-Hamel flow to stretchable convergent/divergent channels. *Computers & Fluids*, 100:196–203.

Usman, M., Haq, R. U., Hamid, M., and Wang, W. (2018). Least square study of heat transfer of water based Cu and Ag nanoparticles along a converging/diverging channel. *Journal of Molecular Liquids*, 249:856–867.